JOURNAL OF AIRCRAFT
Vol. 47, No. 5, September–October 2010

Airfoil Optimization Using Practical Aerodynamic Design Requirements

Howard P. Buckley,* Beckett Y. Zhou,† and David W. Zingg‡
University of Toronto, Toronto, Ontario M3H 5T6, Canada

DOI: 10.2514/1.C000256

Practical aerodynamic design problems must balance the goal of performance optimization over a range of on-design operating conditions with the need to meet design constraints at various off-design operating conditions. Such design problems can be cast as multipoint optimization problems where the on-design and off-design operating conditions are represented as design points with corresponding objective and constraint functions. Two methods are presented for obtaining optimal airfoil designs that satisfy all design objectives and constraints. The first method uses an unconstrained optimization algorithm where the optimal design is achieved by minimizing a weighted sum of the objective functions at each of the operating conditions. To address the competing design objectives between on-design and off-design operating conditions, an automated procedure is used to efficiently weight the off-design objective functions so as to limit their influence on the overall optimization while satisfying the design constraints. The second method uses the constrained optimization algorithm SNOPT, which allows the aerodynamic constraints imposed at the off-design operating conditions to be treated explicitly. Both methods are applied to the design of an airfoil for a hypothetical aircraft where the problem is formulated as an 18-point multipoint optimization. Results are presented confirming that at least two locally optimal solutions exist for this design problem.

Nomenclature

C_1	=	differentiability class of a function whose first derivative is continuous
C	=	off-design constraint function
C_d	=	coefficient of drag
C_l	=	coefficient of lift
$C_{l,\max}$	=	maximum lift coefficient
$C^*_{l,\max}$	=	lower bound on maximum lift coefficient constraint
$\widehat{C}^*_{l,\max}$	=	objective function-specific target maximum lift coefficient
G	=	geometric constraint function
g	=	constraint used in the Kreisselmeier–Steinhauser function
$g_{\max}$	=	maximum Kreisselmeier–Steinhauser constraint value
$\mathbf{g}$	=	vector of Kreisselmeier–Steinhauser constraint values
h	=	weight update formula exponent
j	=	index of flowfield nodes
$\mathcal{J}$	=	objective function
M	=	Mach number
M_{ks}	=	estimate of maximum Mach number in the flowfield given by the Kreisselmeier–Steinhauser function
$M_{\max}$	=	maximum Mach number in the flowfield
$M^*_{\max}$	=	upper bound on maximum Mach number constraint
n	=	index of weight update cycles
N_G	=	number of geometric constraints
p	=	index of on-design objective functions
q	=	index of off-design objective/constraint functions
r	=	index of geometric constraint functions
X	=	design variable vector
X_A	=	design variables at optimal solution A
X_B	=	design variables at optimal solution B
α	=	angle of attack
β	=	step size along vector ΔX
ΔX	=	vector denoting difference in design variables between optimal solutions A and B
μ	=	ℓ_1 penalty function penalty parameter
ρ	=	Kreisselmeier–Steinhauser function draw-down parameter
ϕ_1	=	ℓ_1 penalty function
ψ	=	constraint function used in off-design weight update formula
ψ^*	=	bound on constraint function used in off-design weight update formula
ω	=	objective function weight

Presented as Paper 2009-3516 at the 27th AIAA Applied Aerodynamics Conference, San Antonio, TX, 22–25 June 2009; received 12 January 2010; revision received 30 March 2010; accepted for publication 30 March 2010.

*Research Associate, Institute for Aerospace Studies, 4925 Dufferin Street; howard@oddjob.utias.utoronto.ca. Member AIAA.

†Undergraduate Student, Institute for Aerospace Studies, 4925 Dufferin Street; beckett@oddjob.utias.utoronto.ca. Student Member AIAA.

‡Professor, Institute for Aerospace Studies, 4925 Dufferin Street, Canada Research Chair in Computational Aerodynamics, J. Armand Bombardier Foundation Chair in Aerospace Flight.

I. Introduction

THE aircraft design process applied in industry is a complex endeavor that involves concurrent engineering of the many systems that comprise a fully functional aircraft. In addition to the aerodynamic performance of an aircraft, equal consideration must be given to the disciplines tasked with specifying appropriate structures, controls, materials, and propulsion systems necessary to satisfy a truly comprehensive set of design requirements. In this day and age where greenhouse gas emissions associated with commercial aviation are of public concern with regard to climate change, and rising jet fuel prices are negatively impacting profits of commercial carriers, the design objective of improving aircraft fuel efficiency has become increasingly important. Since aircraft fuel efficiency is directly related to both aerodynamics and weight, the potential for improvements in this area can only be fully realized using a multidisciplinary optimization (MDO) approach. The methods presented in this paper provide a means to consider a broad range of aerodynamic considerations and can be incorporated into an MDO framework.

The coupling of computational fluid dynamics with numerical optimization techniques has resulted in aerodynamic shape optimization algorithms that are efficient at producing aircraft shape configurations with improved performance characteristics at a given aircraft operating condition. While significant progress in the field of aerodynamic shape optimization has been made over the past

20 years, further advancement is still required to make numerical optimization techniques useful to solve practical aerodynamic design problems. Practical aerodynamic design problems are characterized by design requirements that must be satisfied over a broad range of aircraft operating conditions. For aerodynamic shape optimization to be considered a viable alternative to the traditional *cut-and-try* approach to aerodynamic design, it must be capable of producing an optimal design that satisfies the design requirements over this broad range of operating conditions. This type of optimization, in which more than one aircraft operating condition is considered, is commonly referred to as multipoint optimization.

Researchers have addressed the topic of multipoint optimization in various contexts within the realm of aerodynamic design problems [1]. Recently, Epstein et al. [2] used multipoint optimization to minimize wing drag at the main cruise operating condition and nearby secondary cruise operating conditions. Cliff et al. [3] compare two approaches to multipoint optimization as applied to the aerodynamic shape optimization of the Technology Concept Airplane designed by The Boeing Company, simultaneous multipoint design vs sequential cruise-point design followed by trim optimization at transonic conditions. Zingg and Elias [4] as well as Li et al. [5] have used multipoint optimization techniques applied to airfoil design to achieve constant drag over a range of cruise Mach numbers. Li and Padula [6] demonstrate multipoint techniques applied to robust optimization problems which aim to reduce design sensitivity to small changes in uncertain quantities such as Mach number.

Although significant contributions have been made by these researchers and others in the area of multipoint optimization, the scope of its application to aerodynamic design problems has been limited with respect to the range of operating conditions considered. The objective of this paper is to develop a framework for addressing practical aerodynamic design problems that can accommodate the full range of flight conditions that an airplane encounters during a mission. This capability is demonstrated by applying the methodology to the design of an airfoil section for a hypothetical aircraft where the problem is cast as an 18-point multipoint optimization problem. Although this example contains only a portion of the operating conditions that must be considered in the design of an aircraft, it contains a sufficient number of varied on- and off-design conditions to demonstrate the applicability of the methodology to more general problems.

It is now appropriate that we define the terms on-design and off-design as they apply to the practical aerodynamic design problem presented in this paper. In our multipoint optimization problem formulation, on-design points refer to the operating conditions where we wish to optimize aerodynamic performance according to specified design objectives. For example, we may wish to minimize drag over a range of expected cruise Mach numbers and lift requirements. Our off-design points refer to operating conditions that can be considered aerodynamic constraints to the optimization. For example, the off-design requirement that an aerodynamic shape must be able to achieve a specified maximum lift coefficient at low speeds constrains the potential for drag minimization at cruise conditions. Note that the off-design requirements are typically inequality constraints, and there is no benefit to surpassing the specifications.

The work described in this paper follows from the investigation of multipoint optimization applied to practical aerodynamic design problems undertaken by Zingg and Billing [7]. Their goal was to demonstrate that multipoint optimization techniques can be applied to complex aerodynamic design problems that encompass a broad range of requirements extending beyond typical drag minimization over a range of cruise conditions. This broad range of design requirements includes high lift at low speed and consideration of maneuverability under dive conditions. The current work focuses on several key findings from their investigation:

1) Performance at on-design points is compromised by the need to satisfy off-design constraints.

2) On-design performance may be unnecessarily sacrificed if off-design constraints are oversatisfied.

3) Oversatisfaction of off-design constraints can be prevented by appropriate selection of their respective design point weights.

The design point weights mentioned above refer to the weights applied to the respective objective functions in the composite objective function. A problem with multipoint optimization noted by several researchers [4,5] is that the appropriate off-design weights are not known a priori. As implied by the findings of Zingg and Billing, a poor assignment of off-design weights will result in one of two outcomes: 1) the off-design constraints are violated, or 2) the on-design performance is unnecessarily compromised.

One might assume that there is an ideal weight value for any given off-design point that will result in a final optimized shape where its constraint value is exactly satisfied. However, a practical aerodynamic design problem may include off-design points that will have their constraints satisfied regardless of the weight applied to them, referred to as *redundant* points. Given this property of redundant off-design points, their appropriate weight is zero, and they are typically oversatisfied without penalizing performance.

This paper investigates the application of two different methods to solve a practical aerodynamic design problem. The goal of the first method using an unconstrained optimization algorithm is to determine the ideal weights for all of the off-design points considered in a practical aerodynamic design problem in a way that does not require user intervention. We introduce a procedure for automatically obtaining the ideal off-design weights by exploiting aerodynamic performance trends as they evolve throughout the optimization. The second method uses the constrained optimization algorithm SNOPT, which allows the aerodynamic constraints imposed at the off-design operating conditions to be treated explicitly. The off-design points in this method are not included in the composite objective function (which contains only on-design objectives). Rather they are enforced as constraints in conjunction with the composite objective function to define a Lagrangian function that we seek to minimize to find the optimal solution. The following sections characterize, evaluate, and compare these two different approaches to solving practical aerodynamic design problems.

II. Overview Of Optima2D

Both methods make use of the following tools contained within the computational code Optima2D: 1) two-dimensional turbulent flow solver, 2) airfoil geometry parametrization, 3) discrete adjoint gradient calculation, and 4) mesh movement algorithm.

The compressible Reynolds-averaged Navier–Stokes equations are solved at each design iteration with the Newton–Krylov method developed by Nemec and Zingg [8] and Nemec et al. [9], in which the linear system arising at each Newton iteration is solved using the generalized minimal residual method (GMRES) preconditioned with an incomplete lower–upper actorization with limited fill. Spatial derivatives in the governing equations are discretized using second-order centered finite differences with added scalar numerical dissipation. Eddy viscosity is computed using the one-equation Spalart–Allmaras turbulence model. The airfoil geometry is parametrized using B-spline control points. The vertical coordinates of these control points are considered design variables, thus allowing alterations to the baseline shape. For lift-constrained drag minimization problems, the design variables are B-spline control points, and the angle of attack is computed as part of the flow solution to meet the lift constraint (see Zingg and Billing [7] for a description of this treatment of the lift constraint). For lift maximization problems, the angle of attack is a design variable in addition to the B-spline control points. Gradients of objective and constraint functions that are dependent on the flow solution are calculated using the discrete-adjoint method; the adjoint equation is solved using preconditioned GMRES. The computation of the gradient typically requires less than half of the computing time of a flow solution. The first method uses an unconstrained quasi-Newton optimizer in which an estimate of the inverse Hessian based on the BFGS (Broyden–Fletcher–Goldfarb–Shanno) rank-two update formula is used to compute a search direction [10]. The step size is determined using a line search, which enforces the strong Wolfe conditions [10]. The search direction and step size together, determine the new shape of the airfoil (and a new angle of attack in the case of lift maximization). Geometric

constraints are added to the objective function as penalty terms. The second method uses the constrained optimization algorithm SNOPT, which is briefly described in Sec. VI. At each design iteration, the grid around the updated airfoil shape is perturbed using a simple algebraic grid movement technique.

III. Design Problem Definition

To define a practical aerodynamic design problem, a design specification for a hypothetical aircraft is considered[§]. The aircraft has a maximum weight of 100,000 lb, a wing area of 1000ft^2, with a 35-deg sweep. The maximum cruise Mach number of the aircraft is 0.88. The design of the wing section at the mean aerodynamic chord is considered, and it is assumed that the sectional lift coefficient is equal to the wing lift coefficient. The target thickness to chord ratio is 0.12. Regions of the flight envelope considered for this design problem include cruise, long-range cruise, dive, and low-speed conditions.

The first four operating conditions, labeled A-D in Table 1, correspond to cruise. Because of the sweep angle, the effective Mach number is 0.72. Two sets of operating weights and altitudes are considered. For operating point A the altitude is 29,000 ft, the weight is 60,000 lb; for B the altitude is the same, but the weight is 100,000 lb; for C the altitude is 39,000 ft, the weight is 60,000 lb; for D the altitude is 39,000 ft, the weight is 100,000 lb. This leads to the Reynolds numbers and lift coefficients given in Table 1.

The next four operating conditions, labeled E–H, correspond to long-range cruise. The Mach number is 0.78, producing an effective Mach number of 0.64. The altitudes and weights are the same as for A–D, respectively. The vertices of the lower and upper shaded surfaces shown in Fig. 1 are chosen as design points to represent the continuous range of cruise and long-range cruise operating conditions.

The cruise and long-range cruise conditions represented by design points A–H are considered on-design operating conditions. The on-design performance goal for these eight operating conditions is to minimize drag while maintaining their specified lift coefficients. In general, a complete problem specification could involve a careful prioritization of on-design operating conditions based on the knowledge of the aircraft mission requirements. The combination of mission requirements with design objectives may be translated into an objective function defined by a weighted integral which when approximated using a numerical quadrature method provides weights for a finite number of operating conditions. In the present design problem specification, all on-design points are assigned equal importance and thus equal weights.

The next eight operating conditions (I–P) are associated with a safety requirement for maneuverability under dive conditions. The flight Mach number is 0.93, making the effective Mach number 0.76. In addition to the two sets of weights and altitudes considered for the on-design points, two load factors are also taken into account. The combination produces a total of eight dive operating conditions. For operating point I, the altitude is 29,000 ft., the weight 60,000 lbs., and the load factor is 1.3. For operating point J, the altitude and weight are the same, but the load factor is 0.7. Operating points K and L have an altitude of 29,000 ft, a weight of 100,000 lb, and load factors 1.3 and 0.7, respectively. For operating points M and N, the altitude is 39,000 ft, the weight is 60,000 lb, and the load factors are 1.3 and 0.7, respectively. Operating points O and P have the same altitude and load factors, but the weight is 100,000 lb. The dive maneuverability requirement is achieved by keeping shock strengths modest under these conditions, such that the Mach number upstream of a shock is less than or equal to 1.35. Figure 2 shows the vertices of the top shaded surface, which are chosen as design points to represent the continuous range of dive operating conditions.

The final two operating points reflect a safety requirement to be able to achieve an adequate maximum lift coefficient at low-speed conditions. For operating condition Q, the altitude is sea level, the weight is 60,000 lb, and the effective Mach number is 0.16. For operating point R the weight is 100,000 lb, and the effective Mach number is 0.20. The safety requirement specifies that the maximum attainable lift coefficient under these conditions is at least 1.75[¶]. It should be noted that a detailed analysis of the design problem would give consideration to high-lift configurations achieved with the use of slats and flaps. For the sake of simplicity, only single-element airfoils are used to illustrate the methods in this paper.

Table 1 Operating conditions for an 18-point optimization

Operating point	Reynolds number	Mach number	Lift coefficient
A	27.32×10^6	0.72	0.17
B	27.32×10^6	0.72	0.28
C	18.57×10^6	0.72	0.27
D	18.57×10^6	0.72	0.45
E	24.22×10^6	0.64	0.21
F	24.22×10^6	0.64	0.36
G	16.46×10^6	0.64	0.34
H	16.46×10^6	0.64	0.57
I	28.88×10^6	0.76	0.28
J	28.88×10^6	0.76	0.15
K	28.88×10^6	0.76	0.46
L	28.88×10^6	0.76	0.25
M	19.62×10^6	0.76	0.45
N	19.62×10^6	0.76	0.24
O	19.62×10^6	0.76	0.74
P	19.62×10^6	0.76	0.40
Q	11.8×10^6	0.16	-
R	15.0×10^6	0.20	-

The last ten design points, I–R, represent off-design operating conditions. The design requirements at these conditions impose constraints on the optimization. These 18 operating points span the flight envelope. Table 2 summarizes the design objectives and constraints for this design problem. This design problem definition is meant to illustrate a basic set of on-design and off-design specifications that can be used to formulate a multipoint optimization problem. In practice, additional operating conditions, such as climb, also need to be considered, but can be easily accommodated by the methods presented in this paper.

IV. Interpretation of Design Point Weights

There are two terms that are frequently seen in the optimization literature, importance (or priority, of a design point) and difficulty (to improve a design point). Often these two terms are used interchangeably due to their mutual associations with optimization weights. If a design point is considered more important than others, higher weights will be assigned to it. Similarly, a common response to handling a design point that is difficult to improve is to increase its weight, creating the illusion that important points and difficult points should be treated in the same way. However, this multipoint optimization study reveals that it is crucial to distinguish between the two terms and clearly understand their respective influences since the philosophy behind each optimization weight adjustment strategy is shaped by the understanding of these two terms.

Consider the case of a two-point optimization starting at equal weights based on the two points having equal importance and having no prior knowledge of their respective difficulty. After the optimization converges for this hypothetical case, the drag of the first point is reduced by 50% while the drag of the second point is reduced by only 5%. For the next optimization stage, presumably to allow further improvement, one may be tempted to increase the weight on the second point. By doing so, however, the optimization becomes implicitly driven by the difficulty factor. When a point is already in

[§]The design specification was provided by Dr. Tom Nelson at Bombardier Aerospace.

[¶]The optimization procedures applied to this design problem are demonstrated on a coarse mesh. Prior experience has shown that using a lower target lift coefficient of 1.60 on our relatively coarse mesh will yield a lift coefficient of at least 1.75 on a finer mesh.

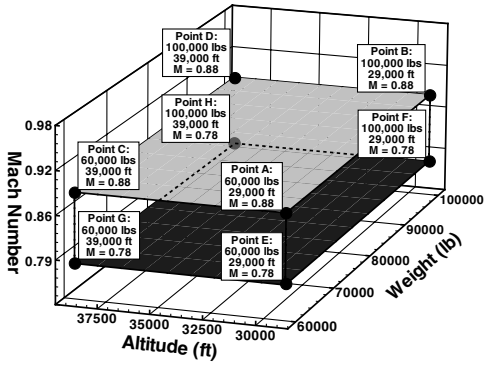

Fig. 1 Visualization of cruise and long-range cruise operating conditions.

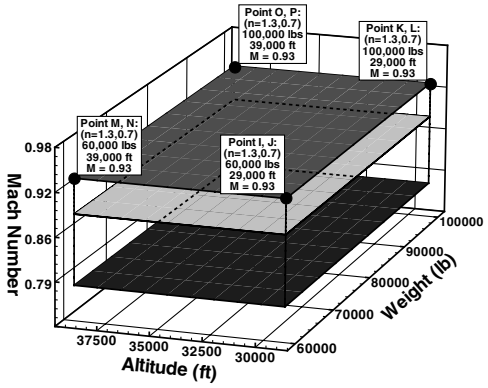

Fig. 2 Visualization of dive operating conditions.

the vicinity of the physical limit to which it can be optimized, the reduction of the objective function will be small. Concentrating on the more difficult point, we forfeit the opportunity to achieve larger overall weighted objective function reduction obtainable by placing equal emphasis on both points based on their having equal importance. The path of the optimization is characterized by sets of optimization weights dictated by the difficulty factor. However this might not be in agreement with the importance factor of each design point. Hence adjusting on-design weights during the optimization based on difficulty is not logical without advanced knowledge of the priorities for the on-design points.

For the off-design points representing aerodynamic constraints the two factors work in harmony. An off-design point whose aerodynamic constraint is the most difficult to improve will be given more weight, implying that it is more important than other off-design points. In this case it is true, since this point is the bottleneck with respect to satisfying the off-design aerodynamic constraints.

V. Strategy for Obtaining Ideal Weights for Off-Design Points (Method 1)

Practical aerodynamic design problems as defined in this paper are by nature constrained optimization problems. The composite objective function used in this method written in terms of on-design and off-design points is given by

$$\mathcal{J} = \sum_{p=1}^{\substack{\#\text{ of}\\ \text{on-design}}} \omega_p^{\text{ON}} \mathcal{J}_p^{\text{ON}} + \sum_{q=1}^{\substack{\#\text{ of}\\ \text{off-design}}} \omega_q^{\text{OFF}} \mathcal{J}_q^{\text{OFF}} \tag{1}$$

The goal of the strategy used in this method is to find the values for the off-design weights ω_q^{OFF} that allow the best possible on-design performance to be achieved while satisfying the off-design constraints. These ideal off-design weights are obtained using an automated weight update procedure that exploits aerodynamic performance trends as they evolve throughout the optimization. The strategy presented in this section employs the unconstrained BFGS optimization algorithm.

The objective function used at on-design points A–H and off-design points I–P is $\mathcal{J}^{\text{ON}} = \mathcal{J}^{\text{OFF}} = C_d$. The lift requirements for these points specified in Table 1 are satisfied using a technique whereby the angle of attack is altered during the iterations of the flow solution such that the desired value of C_l is obtained at convergence. The design variable vector X for this objective function contains only geometric design variables (B-spline control points that define the airfoil geometry).

It is important to note that the off-design constraints are represented as objective functions in this method, as shown in Eq. (1), because they cannot be handled directly by the BFGS algorithm. The off-design constraints are satisfied indirectly by minimizing objective functions known to correlate with the constraint values. For example, the off-design constraints at operating points I–P are given by $M_{\max} \leq 1.35$. The upstream Mach number near a shock on the airfoil has a loose correlation to the drag coefficient. By reducing the drag coefficient, the maximum Mach number in the flowfield is also reduced. Therefore, the objective function representing these off-design constraints is given by $\mathcal{J}^{\text{OFF}} = C_d$. At off-design points where $M_{\max} > 1.35$, the corresponding off-design weights are adjusted so that C_d is reduced just enough to satisfy the $M_{\max}$ constraint value at exactly 1.35.

The same logic is applied to the high-lift constraints at off-design points Q and R where the constraints are given by $C_{l,\max} \geq 1.60$. In this case, the objective function representing these constraints is given by

$$\mathcal{J}^{\text{OFF}} = \left(1 - \frac{C_{l,\max}}{\widehat{C}^*_{l,\max}}\right)^2 \tag{2}$$

where $\widehat{C}^*_{l,\max}$ is a target maximum lift coefficient specific to the objective function not to be confused with the lower bound on the maximum lift coefficient constraint, $C^*_{l,\max}$ [see Eq. (5) used in the weight update formula]. The value of $\widehat{C}^*_{l,\max}$ is set to a value that is unattainable and hence this corresponds to lift maximization. The optimization algorithm will strive to attain the objective-function-specific target lift value $\widehat{C}^*_{l,\max}$ at points Q and R, while their corresponding weights will be adjusted to ensure that $C_{l,\max} \geq C^*_{l,\max}$. For this lift maximization objective function, the angle of attack, α, is a design variable in addition to the geometric design variables.

Table 2 Design objectives and constraints for an 18-point optimization

Operating point	Operating condition	On-design objective	Off-design constraint
A–D	Cruise	Lift-constrained drag minimization	——
E–H	Long-range cruise	Lift-constrained drag minimization	——
I–P	Dive	——	$M_{\max} \leq 1.35$
Q–R	Low speed	——	$C_{l,\max} \geq 1.60$

A. On-Design-First Optimization

In this approach, the procedure begins with an optional start-up optimization. The term on-design-first refers to this start-up optimization, which includes only the on-design points. Performing an initial optimization with only on-design operating points serves two purposes. First, it gives a clear picture of the performance tradeoffs associated with the off-design constraints. Second, the initial airfoil may be poorly suited to the off-design operating points, which may cause flow solver convergence difficulties. In such cases, performing the on-design-first optimization typically provides a better starting shape for introducing the off-design points. The resultant airfoil geometry from the on-design-first optimization minimizes a weighted sum of the objective functions at all on-design

points. Under the assumption that all of the on-design operating conditions are of equal importance, all on-design objective functions are weighted equally; however the weight assignment is ultimately at the discretion of the designer, who may choose to weight the on-design points differently according to design priorities. This on-design-first airfoil is the starting point for the main optimization procedure that includes both the on-design points and the off-design points.

In cases where the initial airfoil geometry does not cause flow solver convergence difficulties at any of the off-design points, the on-design-first optimization may be unnecessary. Moreover, the method is likely to be more efficient if the on-design first optimization can be omitted.

B. Weight Update Formula

For any given off-design point, there are 3 possibilities for the value of its respective aerodynamic constraint: 1) the constraint is violated, 2) the constraint is exactly satisfied, and 3) the constraint is oversatisfied.

For off-design points where the constraints are violated, a higher weight is required on these points to pull them into the feasible region of the design space. For off-design points where the constraints are exactly satisfied, the weight is appropriate and does not require modification. For off-design points where constraints are oversatisfied, a lower weight is required to allow them to drift toward the boundary of the feasible region of the design space. As there is no particular benefit to oversatisfying an off-design constraint, it is desirable to shed weight on the off-design points that are in this category to reduce the negative impact on on-design performance. To facilitate the modification of off-design weights, a simple weight update formula is employed.

The concept for this approach to off-design weight modification can be credited to the work of Zingg and Elias [4] that demonstrates a similar technique for obtaining equal drag coefficients across a range of cruise Mach numbers by altering the objective function weights of design points in a multipoint optimization. For an off-design constraint given by $\psi \leq \psi^*$, where ψ is some functional, the weight update formula used in our procedure is

$$\omega_{n+1} = \omega_n \left(\frac{\psi_n}{\psi^*} \right)^h \tag{3}$$

where ψ_n is the current off-design constraint value, ω_n and ω_{n+1} are the current and updated off-design weights, the exponent h is a user defined parameter that affects the magnitude of the weight change, and n is the index of weight update cycles.

For off-design points representing requirements for $C_{l,\max}$, the values of ψ_n and ψ^* to be used in the weight update formula are

$$\psi_n = \frac{1}{C^n_{l,\max}} \tag{4}$$

$$\psi^* = \frac{1}{C^*_{l,\max}} \tag{5}$$

For off-design points with a maximum local Mach number constraint, $M_{\max} \leq M^*_{\max}$, the values of ψ_n and ψ^* to be used in the weight update formula are

$$\psi_n = M^n_{\max} \tag{6}$$

$$\psi^* = M^*_{\max} \tag{7}$$

The first application of the weight update formula to obtain initial off-design weights ω_1 requires special treatment because there are no previous weights to use in the formula. An arbitrary value of unity is assigned to ω_0 for all off-design points. The off-design constraint values ψ_0 are evaluated using the initial airfoil geometry. Initial off-design weights ω_1 are then calculated using the weight update formula with $\omega_0 = 1$. It is important to clarify that the ω_0 weights are not used at any time during the optimization procedure; they only facilitate the calculation of ω_1. The weight update formula is subsequently used at regular intervals (after every weight update cycle) throughout the main optimization procedure to update the off-design weights.

C. Weight Update Cycles

The weights of the off-design points are updated periodically based on the values of their respective constraints during the course of the optimization. A weight update cycle consists of a user-specified number of optimization iterations followed by an evaluation of the off-design constraints and corresponding update of the off-design weights. A new weight update cycle begins with a restarted optimization using the updated off-design weights and the final airfoil geometry from the previous weight update cycle. If the magnitude of the change in the updated weights is less than a user-specified tolerance, the optimization leaves the weights unchanged and continues until the next weight update cycle. In this manner, weight update cycles are executed until a converged optimal solution is obtained. At the converged optimal solution, the off-design weights are as low as possible while satisfying all of the off-design constraints.

VI. Alternative Strategy Using Constrained Optimization (Method 2)

An alternative strategy for solving practical aerodynamic design problems uses the SNOPT algorithm for constrained optimization problems developed by Gill et al. [11]. The SNOPT algorithm allows us to treat the off-design operating conditions as explicit constraints within the framework of a constrained optimization problem. SNOPT uses a sequential quadratic programming (SQP) method that obtains search directions from a sequence of quadratic programming (QP) subproblems. Each QP subproblem minimizes a quadratic model of a Lagrangian function which is used to represent an objective function subject to linearized constraints.

A. On-Design-First Optimization with SNOPT

As with the off-design weight update strategy, it may be necessary to perform an on-design-first optimization to obtain a favorable airfoil geometry for use as a starting point before the introduction of the off-design constraints. In such cases SNOPT is used to minimize a weighted sum of the objective functions at all on-design points. This composite objective function is subject only to geometric thickness constraints which are satisfied explicitly by SNOPT.

B. KS Function Used for Evaluation of Maximum Mach Number Constraints

Off-design points I-P representing dive conditions are subject to the constraint that the maximum Mach number in the flowfield not exceed 1.35. The maximum Mach number function used to represent this constraint is not continuous with respect to the design variables and therefore cannot be handled directly by SNOPT. Since the Mach number at each node is continuous with respect to the design variables, we could assign the Mach number constraint to each node in the flowfield. However, performing an adjoint gradient evaluation of the Mach number constraint at each node would be prohibitively expensive. Instead we use the Kreisselmeier–Steinhauser (KS) function [12] as a means to aggregate the Mach number constraints at all nodes in the flowfield into a single composite function that is continuously differentiable. The KS function produces an envelope surface that is C_1 continuous and represents a conservative estimate of the maximum among the set of constraint functions considered [13]. The KS function has been used in various applications where constraint aggregation is required for efficient use of gradient-based optimization methods including aerodynamic shape optimization [14] and aircraft design [15–17]. An alternate formulation of the KS function proposed by Wrenn [13] is used to reduce numerical difficulties associated with the original formulation and is given by

$$\mathrm{KS}[\mathbf{g}(X)] = g_{\max}(X) + \frac{1}{\rho}\ell_n\left[\sum_{j=1}^{m} e^{\rho[g_j(X)-g_{\max}(X)]}\right] \tag{8}$$

where $\mathbf{g}(X)$ contains the set of constraints, $g_{\max}$ is the maximum constraint value evaluated at the current design iteration, X, and ρ is the draw-down parameter that governs the conservativeness of the estimate of $g_{\max}$ such that

$$\lim_{\rho\to\infty} \mathrm{KS}(X,\rho) = g_{\max}(X) \tag{9}$$

The constraints $g_j(X)$ are evaluated at every node in the flowfield with the exception of the nodes on the surface of the airfoil and are given by

$$g_j(X) = \frac{M_j(X)}{M^*_{\max}} - 1 \tag{10}$$

where $M^*_{\max} = 1.35$ is the upper bound on the Mach number constraint, $M_j(X)$ is the Mach number at node j at the current design iteration, X, and the constraint is considered satisfied if $g_j(X) \le 0$. $g_{\max}$ is given by

$$g_{\max}(X) = \frac{M_{\max}(X)}{M^*_{\max}} - 1 \tag{11}$$

where $M_{\max}(X)$ is the maximum Mach number in the flowfield at the current design iteration X.

A conservative estimate of the maximum Mach number is given by:

$$M_{\mathrm{ks}}(\mathrm{KS}) = (\mathrm{KS}+1)M^*_{\max} \tag{12}$$

The actual constraint that SNOPT works with is M_{ks}. To obtain a solution that satisfies the desired maximum Mach number constraint, $M_{\max} \le M^*_{\max}$, appropriate values of ρ and the M_{ks} target must be specified and are case dependent. Currently, an ad hoc approach is taken to determine these values.

C. Evaluation of High-Lift Constraints

Off-design points Q-R representing design requirements for high lift at low speeds are subject to the constraint that $C_{l,\max}$ must be at least 1.60. The constraint function assigned to these points is given simply as C_l.

D. Off-Design Constraint Function Gradients

The gradients of the constraint functions M_{ks} and C_l with respect to the design variables, X, are computed using the discrete adjoint approach.

VII. Results

A. Multipoint Optimization Setup

For all cases, the airfoil geometry is parametrized using 15 B-spline control points. Unless otherwise specified, one control point is frozen at the leading edge and two at the trailing edge. The remaining 12 control points are designated as design variables and are split evenly between the top and bottom airfoil surfaces. Thickness constraints of 1 and 0.2% chord are imposed at 95 and 99% chord, respectively, to prevent trailing-edge crossover. The latter is typically inactive once convergence is achieved. In addition, case-specific floating thickness constraints are described in the following sections. The base grid used in all cases has a C topology with 289 nodes in the streamwise direction and 65 nodes in the normal direction; the off-wall spacing is 2×10^{-6} chord. It was created using the RAE 2822 airfoil geometry. Cases 1 to 3 use the off-design weight update method described in Sec. V. Case 4 and cases A and B use the constrained optimization method described in Sec. VI.

The flow solver described in Sec. II is used to evaluate airfoil performance in all cases. Given studies of the flow solver's accuracy performed by Zingg [18] and Zingg et al. [19], the grids used can be expected to predict lift coefficients accurate to within 1% and drag coefficients to within 5% for attached and mildly separated flows, including both numerical and physical model error.

1. *Off-Design Weight Update Setup for Cases 1–3*

For design points A through P, the design objective is lift-constrained drag minimization. For each of these design points, the corresponding objective function is given by $\mathcal{J} = C_d$. For design points Q and R, the design objective is to meet minimum $C_{l,\max}$ requirements needed at low speeds. A value of 2.0 is used for $\widehat{C}^*_{l,\max}$ in the high-lift objective function Eq. (2). Off-design objective functions at design points I-R are used to satisfy corresponding off-design constraints as described in Sec. V. The objective functions at all design points are normalized by their respective objective function values obtained using the initial airfoil geometry. The weights for the on-design points A–H remain fixed at unity throughout the duration of the optimization procedure. The weights for the off-design points I-R are periodically modified throughout the optimization procedure according to the strategy described in Sec. V. Ten optimization iterations are executed per weight update cycle. The value of the exponent used in the weight update formula, Eq. (3), is $h = 4$. This choice leads to adequate convergence behavior but has not been studied extensively, so other values may be preferable in some cases. Convergence for an optimization performed using the off-design weight update procedure is achieved when the change in the sum of on-design drag coefficients over six consecutive weight update cycles is less than 10^{-4}, and all off-design constraints are satisfied. Because the penalty method used to handle constraints allows for small violations, a floating thickness constraint of 12.06% is imposed to ensure a thickness of at least 12% chord.

2. *Constrained Optimization Setup for Case 4 and Local Minima Cases*

For on-design points A–H, the design objective is lift-constrained drag minimization. For each of these design points, the corresponding objective function is the drag coefficient normalized by the drag coefficient evaluated using the initial airfoil geometry. A composite objective function is formed by a weighted sum of the individual on-design objective functions with all weights equal to unity. The off-design constraints are defined as described in Sec. VI. A value of $\rho = 31.45$ is used in the KS function. The target value of M_{ks} used by SNOPT is 1.50. Experiments were performed to determine the values of M_{ks} and ρ which produce $M_{\max} \le 1.35$ as desired (Sec. VI.B). Unlike the penalty method used for handling constraints in cases 1–3, thickness constraints in case 4 and the local minima cases are satisfied exactly by SNOPT. Therefore, for case 4, the floating thickness constraint of 12.0002% chord is based on the thickness of the optimized geometry obtained from case 1 to ensure an accurate comparison between these two cases. For the local minima cases, a floating thickness constraint of 11.857% is used.

B. Case 1: Baseline 18 Point Optimization (Optimized RAE 2822 Airfoil)

The initial geometry used for the optimization in this case is the RAE 2822 airfoil. The practical aerodynamic design problem is solved using the off-design weight update procedure with the full set of 18 design points, A-R, described in Table 1.

The results for case 1 presented here were obtained after 27 weight update cycles, or approximately 400 function evaluations (flow solutions) per operating condition. Figure 3 shows the optimized airfoil from case 1 compared with the initial RAE 2822 airfoil. Tables 3 and 4 provide a summary of the on-design and off-design performance values for the initial RAE 2822 airfoil and the airfoil

Fig. 3 Optimized RAE 2822 airfoil versus initial RAE 2822 airfoil.

after 27 weight update cycles. Note that for the RAE 2822 airfoil the off-design constraints at points O, Q, and R, shown in bold text, are violated. A comparison of the drag coefficients at the on-design points for the final optimized airfoil versus the RAE 2822 airfoil shows that there has been degradation in performance, but the severity of the degradation has been mitigated by use of the automated weight update procedure. The penalty incurred in on-design performance is the price paid to satisfy the off-design constraints. Pressure distributions for all on-design points A–H are shown in Figs. 4 and 5. The solutions are shock free at all eight on-design operating conditions.

1. *Off-Design Points*

Figures 6 and 7 show the evolution of the constraint values for off-design points I-P and Q and R, respectively, throughout the optimization procedure. Figure 8 shows corresponding off-design weights. At the beginning of the optimization procedure, the off-design constraints are violated at points O, Q, and R, while the remaining off-design constraints are satisfied. Since some off-design constraints are not satisfied, we must proceed with the weight update cycles, which will result in degradation in on-design performance. The off-design weights begin at their initial reference values of unity. Within the first several weight update cycles, two distinct categories of off-design points emerge from these plots: 1) active off-design points, and 2) redundant off-design points.

Points O, Q, and R can be considered active. These points require nonzero weights to prevent violation of their target constraint values. It is clear from Fig. 8 that the off-design constraint at point O is the most difficult to satisfy, as illustrated by its high weight compared with the other active points Q and R. Points J, I, K, L, M, N, and P can be considered redundant. These points will have their constraints satisfied regardless of the weight applied to them. Redundant points have their constraints satisfied by virtue of their proximity to active points with similar operating conditions. The weight update strategy recognizes this property of the redundant off-design points and accordingly reduces their weights to zero, as shown in Fig. 8.

The behavior of the active off-design points is characterized by an initial period of growth followed by asymptotic convergence of their constraints to their respective target values with corresponding constant weight values. The redundant points attain constant over-satisfied constraint values with corresponding weightings of zero. This behavior is observed in Figs. 6–8.

It is likely that point Q is also redundant. Throughout the optimization procedure, the off-design constraint value at point Q, $C_{l,\max}$, follows slightly above the $C_{l,\max}$ constraint value at point R, as shown in Fig. 7. It appears that as long as the $C_{l,\max}$ constraint at point R is satisfied, the $C_{l,\max}$ constraint at point Q will also be satisfied with a slightly higher value. The claim of redundancy of point Q can be further justified by noting that its weight is slowly approaching zero while the weight on point R remains constant during the last 10 weight update cycles. It is reasonable to assume that if the optimization were allowed to continue beyond 27 weight update cycles, the weight for point Q would eventually reach zero.

2. *On-Design Points*

Since the on-design optimization weights are held constant throughout the optimization procedure, the on-design performance is evolving through the course of the optimization solely due to the shift of emphasis characterized by the relative change in the off-design weights. Figure 9 shows the evolution of the drag coefficients for the eight on-design points. In the first 7 weight update cycles, some on-design performance fluctuation is observable. With the introduction of the off-design points, the on-design drag values immediately begin to rise. Figure 10 shows the sum of the on-design drag coefficients

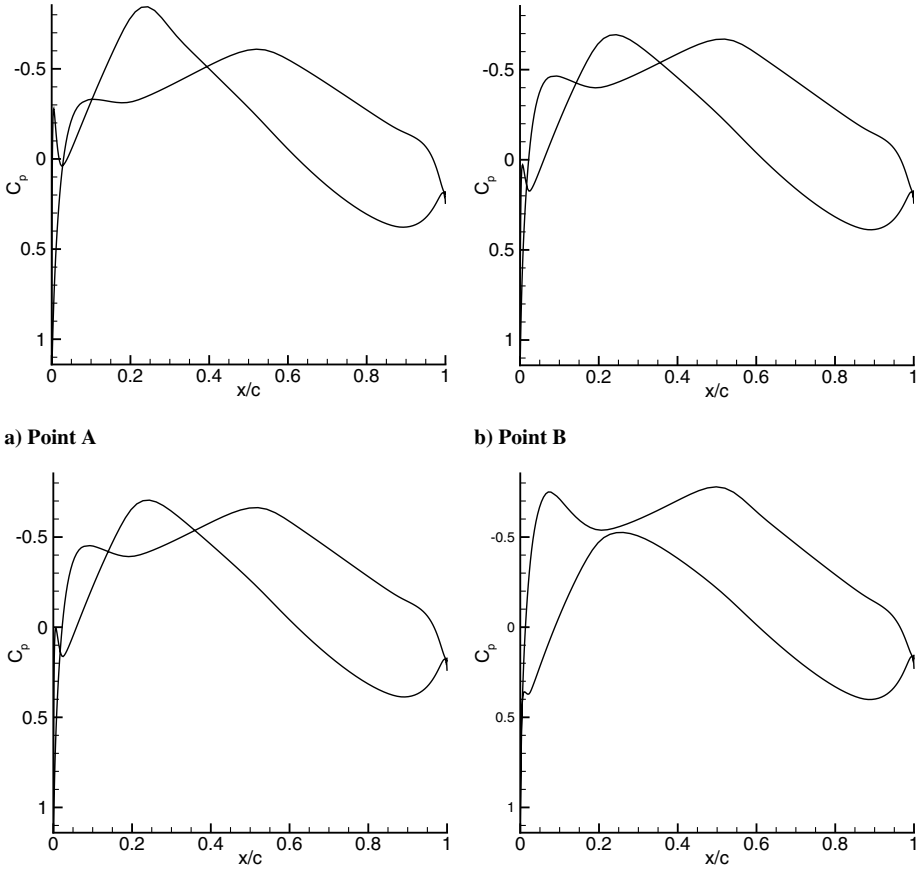

Fig. 4 Surface pressure coefficient distributions for operating points A-D (RAE 2822 optimized airfoil).

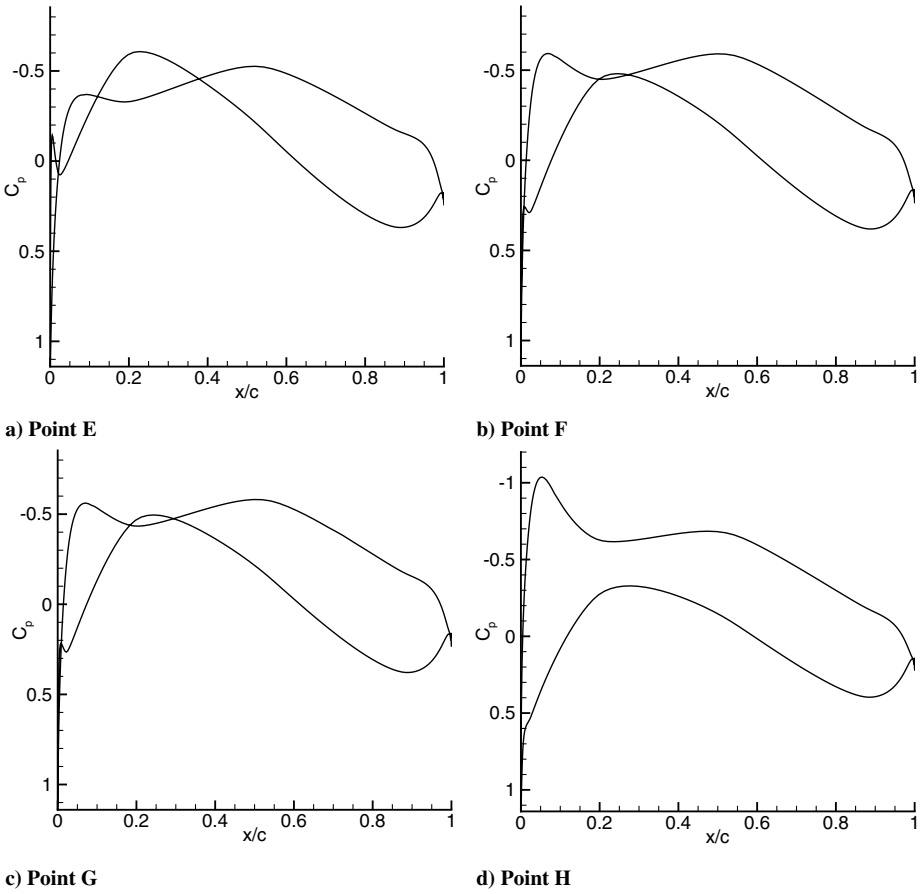

Fig. 5 Surface pressure coefficient distributions for operating points E-H (RAE 2822 optimized airfoil).

superimposed against the sum of the off-design weights. It illustrates the relationship between on-design performance and off-design weights.

C. Case 2: Alternate Initial Airfoil (Optimized NACA 0012 Airfoil)

The initial geometry used for the optimization in this case is the NACA 0012 airfoil, which is a symmetrical airfoil, in contrast to the RAE 2822 supercritical airfoil used in case 1. The initial grid is found by using the grid movement algorithm to alter the grid generated around the RAE 2822 airfoil for case 1 to conform to the NACA 0012 airfoil. This ensures that despite the different initial airfoils, the grid produced around a given geometry is the same for Cases 1 and 2. An on-design-first optimization is performed followed by the main optimization employing the off-design weight update procedure using the full set of 18 design points, A-R, described in Table 1.

The results shown were obtained after 45 weight update cycles. A comparison of the optimized NACA 0012 airfoil obtained in case 2 versus the optimized RAE 2822 airfoil obtained in case 1 is shown in Fig. 11. Table 5 shows a comparison of the performance values for the final optimized airfoil for case 2 versus the initial NACA 0012 airfoil performance values. Although the on-design performance for case 2 is comparable to case 1, significant differences are observed in off-design performance and airfoil geometry. In spite of these differences, the off-design weight update procedure has produced a converged solution for case 2 according to the definition provided in Sec. VII.A.1. As further described in Sec. VII.F, the solutions to cases 1 and 2 are examples of two locally optimal solutions. In the presence of local optima, the initial geometry becomes important. The RAE 2822, being a supercritical airfoil, is a better choice than the symmetric NACA 0012 section. Furthermore, the optimization converged more rapidly when initialized with the RAE 2822 airfoil.

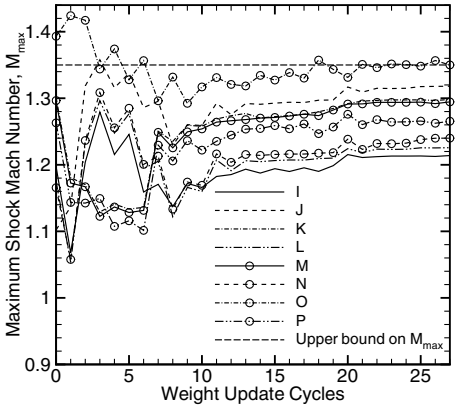

Fig. 6 Evolution of off-design constraint values I-P.

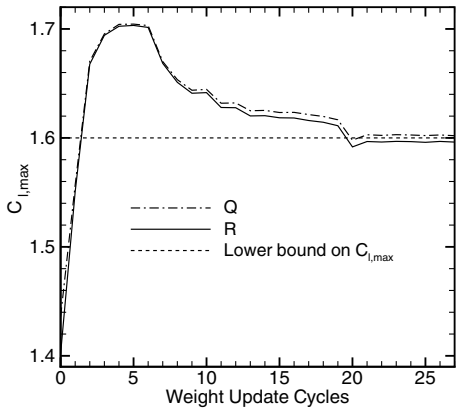

Fig. 7 Evolution of off-design aerodynamic constraint values Q and R.

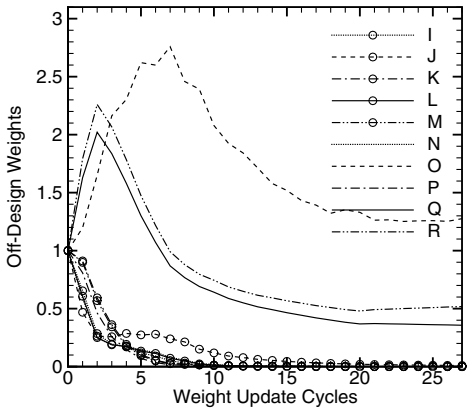

Fig. 8 Evolution of off-design weights.

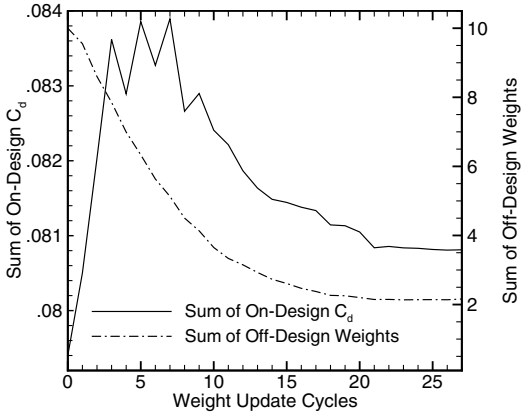

Fig. 10 Sum of on-design performance values versus sum of off-design weights.

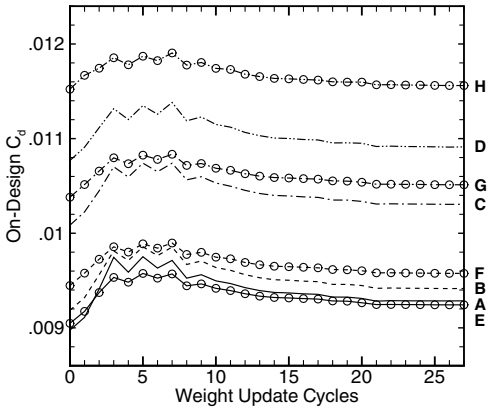

Fig. 9 Evolution of on-design performance.

D. Case 3: Reduced Set of Off-Design Points

The initial geometry used for the optimization in this case is the RAE 2822 airfoil. A reduced set of design points is used. On-design points A-H are included, but only off-design points O and R are included for a total of 10 design points. The results from case 1 revealed that the other off-design points are redundant.

Table 6 shows the performance values for the optimized airfoil obtained after 26 weight update cycles and a comparison of the optimized airfoil geometries from case 3 versus case 1 are shown in Fig. 12. These results show that the final airfoil geometry and performance values for case 3 are nearly identical to results obtained for case 1. In practice, the knowledge regarding the redundancy of the off-design points would not be available before running the optimization. However it is instructive to show that the same optimized results are obtained with significantly less computational effort. Both cases required a similar number of design iterations and weight update cycles, but only 10 flow solutions and adjoint calculations per design iteration were required for this case compared with 18 for case 1. To improve computational efficiency, criteria for determining redundancy of design points during the optimization procedure could be incorporated into the method, providing the opportunity to eliminate analysis of such points and the associated computing cost.

E. Case 4: Full Set of Off-Design Points Using SNOPT

Case 4 repeats case 1 but using the constrained optimization method instead of the off-design weight update method. The results for case 4 were obtained after 52 function evaluations (flow solutions) per operating condition. The optimized solution satisfies the first-order optimality conditions for a constrained optimization problem. On-design performance has been optimized while all off-design constraints have been satisfied. A comparison of the performance results shown in Table 7 versus the performance results for case 1 shown in Table 4 reveals that the on-design and off-design performance is very similar in both cases. Figure 13 shows that the optimized airfoil geometries for cases 1 and 4 are also very similar. Convergence using the SNOPT method is achieved with substantially less computational effort than that required for the

Table 3 RAE 2822 airfoil performance

Operating point	α	C_l	C_d	$M_{\max}$	$C_{l,\max}$
A	−0.71°	0.17	0.0090	——	——
B	−0.06°	0.28	0.0092	——	——
C	−0.12°	0.27	0.0101	——	——
D	+0.93°	0.45	0.0108	——	——
E	−0.36°	0.21	0.0090	——	——
F	+0.66°	0.36	0.0094	——	——
G	+0.53°	0.34	0.0104	——	——
H	+2.10°	0.57	0.0115	——	——
I	−0.17°	0.28	0.0100	1.20	——
J	−0.85°	0.15	0.0092	1.10	——
K	+0.87°	0.46	0.0136	1.30	——
L	−0.33°	0.25	0.0097	1.17	——
M	+0.77°	0.45	0.0141	1.30	——
N	−0.39°	0.24	0.0105	1.16	——
O	+3.46°	0.74	0.0383	1.40	——
P	+0.48°	0.40	0.0128	1.26	——
Q	+16.50°	——	——	——	1.43
R	+16.50°	——	——	——	1.40

Table 4 Optimized RAE 2822 airfoil performance after 27 weight update cycles (case 1)

Operating point	α	C_l	C_d	$M_{\max}$	$C_{l,\max}$
A	−1.26°	0.17	0.0093	——	——
B	−0.63°	0.28	0.0094	——	——
C	−0.67°	0.27	0.0103	——	——
D	+0.38°	0.45	0.0109	——	——
E	−1.00°	0.21	0.0092	——	——
F	+0.03°	0.36	0.0096	——	——
G	−0.09°	0.34	0.0105	——	——
H	+1.49°	0.57	0.0116	——	——
I	−0.66°	0.28	0.0110	1.21	——
J	−1.33°	0.15	0.0120	1.32	——
K	+0.36°	0.46	0.0138	1.30	——
L	−0.82°	0.25	0.0110	1.23	——
M	+0.31°	0.45	0.0143	1.29	——
N	−0.86°	0.24	0.0118	1.24	——
O	+1.87°	0.74	0.0209	1.35	——
P	+0.01°	0.40	0.0133	1.27	——
Q	+14.92°	——	——	——	1.60
R	+14.70°	——	——	——	1.60

Fig. 11 Optimized NACA 0012 airfoil versus optimized RAE 2822 airfoil.

Fig. 12 Optimized RAE 2822 airfoil optimized with reduced set of off-design points versus optimized RAE 2822 airfoil using full set of 18 design points.

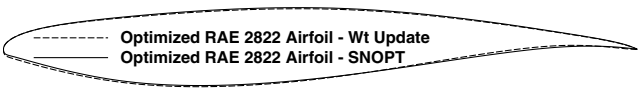

Fig. 13 Comparison of optimized airfoils obtained using the SNOPT method and the off-design weight update method.

Fig. 14 A comparison of two locally optimal airfoil geometries.

off-design weight update method given that the final solution of case 4 was achieved approximately eight times faster than for case 1.

F. The Existence of Multiple Local Minima

The results presented in this section confirm the existence of at least two locally optimal solutions to the design problem described in Sec. III. Both solutions satisfy the first order optimality conditions for a constrained optimization problem, yet the solutions exhibit dramatic differences in geometry and performance.

The two solutions were obtained using the SNOPT constrained optimization method described in Sec. VI. The optimization input parameters in each case are identical with the exception of the initial airfoil geometry. Both cases use the same base grid, which ensures that the underlying grid properties are consistent. Case NACA begins with the base grid initially perturbed to conform to the NACA 0012 airfoil geometry, whereas case RAE begins with the base grid perturbed to conform to the RAE 2822 airfoil geometry. A comparison of the final optimized airfoil geometries for cases NACA and RAE is shown in Fig. 14. Table 8 shows a comparison of the final optimized performance values for cases NACA and RAE.

To illuminate the character of the local optimal solutions obtained in cases NACA and RAE, the objective and constraint functions are evaluated at points along a vector, ΔX, connecting the two sets of design variables that define the optimal airfoil geometries. Each point represents an intermediate airfoil geometry between the two optimal geometries. The design variables at the intermediate points are interpolated between the design variables at case NACA and case RAE as

$$X(\beta) = X_{\text{NACA}} + \beta[\Delta X] \tag{13}$$

$$\Delta X = X_{\text{RAE}} - X_{\text{NACA}} \tag{14}$$

with X_{NACA} and X_{RAE} representing the design variables for the final airfoil geometries of cases NACA and RAE, respectively. Therefore, $\beta = 0$ and $\beta = 1$ correspond to case NACA and case RAE, respectively.

A merit function that combines the objective function with measures of constraint violation can be plotted to show the optimal solutions as stationary points along ΔX. The merit function used to visualize the behavior of the objective and constraint functions near the optimal solutions is the ℓ_1 penalty function, defined as

$$\phi_1(X) = \sum_{p=1}^{\substack{\#\text{ of}\\ \text{on-design}}} \mathcal{J}_p(X) + \mu \sum_{q=1}^{\substack{\#\text{ of}\\ \text{off-design}}} [C_q(X)]^- + \mu \sum_{r=1}^{N_G} [G_r(X)]^- \tag{15}$$

where the first term represents the objective function, which is the sum of drag coefficients at the on-design operating conditions, and the second and third terms represent weighted sums of off-design and geometric constraint violations, respectively. Constraint violations are added as penalties to the objective function. The notation $[z]^- = \max\{0, -z\}$ is used to indicate that a satisfied constraint does not contribute to its penalty term. The positive scalar μ is the penalty parameter. It must be noted that the ℓ_1 penalty function is considered to be an exact merit function because it has the important property

Table 5 Optimized NACA 0012 airfoil performance versus NACA 0012 airfoil performance

Operating point	NACA 0012					Optimized NACA 0012 airfoil				
	α	C_l	C_d	$M_{\max}$	$C_{l,\max}$	α	C_l	C_d	$M_{\max}$	$C_{l,\max}$
A	+1.01°	0.17	0.0092	——	——	−1.42°	0.17	0.0093	——	——
B	+1.67°	0.28	0.0105	——	——	−0.77°	0.28	0.0094	——	——
C	+1.61°	0.27	0.0111	——	——	−0.82°	0.27	0.0103	——	——
D	+2.82°	0.45	0.0188	——	——	+0.23°	0.45	0.0110	——	——
E	+1.45°	0.21	0.0093	——	——	−1.14°	0.21	0.0093	——	——
F	+2.48°	0.36	0.0100	——	——	−0.11°	0.36	0.0096	——	——
G	+2.35°	0.34	0.0108	——	——	−0.23°	0.34	0.0105	——	——
H	+3.95°	0.57	0.0136	——	——	+1.36°	0.57	0.0115	——	——
I	+1.57°	0.28	0.0160	——	——	−0.80°	0.28	0.0112	1.25	——
J	+0.81°	0.15	0.0110	——	——	−1.51°	0.15	0.0100	1.17	——
K	+3.06°	0.46	0.0337	1.47	——	+0.28°	0.46	0.0150	1.31	——
L	+1.38°	0.25	0.0146	1.32	——	−0.97°	0.25	0.0108	1.23	——
M	+2.92°	0.45	0.0326	1.46	——	+0.22°	0.45	0.0155	1.31	——
N	+1.33°	0.24	0.0149	1.32	——	−1.02°	0.24	0.0115	1.22	——
O	+15.50°	0.74	0.2545	1.68	——	+1.81°	0.74	0.0219	1.35	——
P	+2.42°	0.40	0.0261	1.42	——	−0.09°	0.40	0.0142	1.30	——
Q	+15.00°	——	——	——	1.45	+14.78°	——	——	——	1.60
R	+15.00°	——	——	——	1.44	+14.62°	——	——	——	1.60

Table 6 Performance of optimized RAE 2822 airfoil with reduced set of off-design points

Operating point	α	C_l	C_d	$M_{\max}$	$C_{l,\max}$
A	−1.34°	0.17	0.0093	——	——
B	−0.70°	0.28	0.0094	——	——
C	−0.75°	0.27	0.0103	——	——
D	+0.31°	0.45	0.0109	——	——
E	−1.07°	0.21	0.0093	——	——
F	−0.04°	0.36	0.0096	——	——
G	−0.17°	0.34	0.0105	——	——
H	+1.41°	0.57	0.0116	——	——
I	−0.73°	0.28	0.0110	1.21	——
J	−1.41°	0.15	0.0122	1.32	——
K	+0.29°	0.46	0.0137	1.29	——
L	−0.89°	0.25	0.0110	1.23	——
M	+0.23°	0.45	0.0142	1.29	——
N	−0.94°	0.24	0.0118	1.25	——
O	+1.81°	0.74	0.0210	1.35	——
P	−0.07°	0.40	0.0131	1.27	——
Q	+14.90°	——	——	——	1.60
R	+14.73°	——	——	——	1.60

Table 7 Performance of optimized RAE 2822 airfoil obtained using the SNOPT method

Operating point	α	C_l	C_d	$M_{\max}$	M_{ks}	$C_{l,\max}$
A	−1.47°	0.17	0.0093	——	——	——
B	−0.84°	0.28	0.0094	——	——	——
C	−0.89°	0.27	0.0103	——	——	——
D	+0.15°	0.45	0.0109	——	——	——
E	−1.21°	0.21	0.0092	——	——	——
F	−0.20°	0.36	0.0095	——	——	——
G	−0.32°	0.34	0.0105	——	——	——
H	+1.25°	0.57	0.0115	——	——	——
I	−0.86°	0.28	0.0113	1.23	1.39	——
J	−1.53°	0.15	0.0122	1.32	1.44	——
K	+0.16°	0.46	0.0145	1.30	1.44	——
L	−1.02°	0.25	0.0113	1.24	1.39	——
M	+0.11°	0.45	0.0150	1.30	1.43	——
N	−1.06°	0.24	0.0121	1.24	1.39	——
O	+1.75°	0.74	0.0224	1.34	1.50	——
P	−0.19°	0.40	0.0138	1.28	1.42	——
Q	+14.56°	——	——	——	——	1.60
R	+14.48°	——	——	——	——	1.60

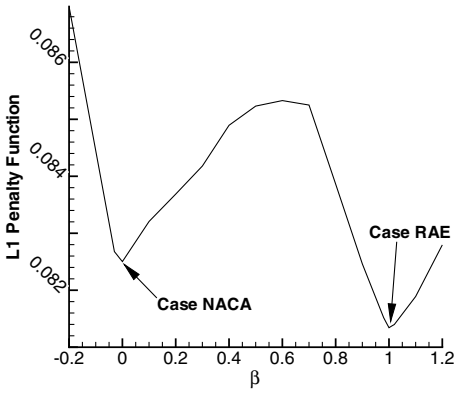

Fig. 15 The ℓ_1 penalty function in the vicinity of solutions for cases NACA and RAE.

that for an appropriately selected value of μ, any locally optimal solution of the constrained optimization problem is also a local minimizer of ϕ_1 [10]. Figure 15 shows the behavior of the ℓ_1 penalty function along the direction ΔX in the vicinity of the solutions for cases NACA and RAE. Two local minima can be seen at $\beta = 0$ and $\beta = 1$ which correspond to the final airfoil geometries of Cases NACA and RAE, respectively. The solution for case RAE is clearly superior because it has a lower objective function value, or in practical design terms, it has a lower sum of on-design drag coefficients. Case RAE also attains lower values of the M_{ks} off-design constraints where it can be seen in Table 8 that only the M_{ks} constraint at point O is active, compared with case NACA where the M_{ks} constraints at points J, K, M, O, and P are active or near-active. The juxtaposition of the active constraint functions against the objective function shown in Figs. 16a–16c typifies the nature of optimal solutions to a constrained optimization problem. These figures highlight the role that the active constraints play in determining the local optimal solutions in Cases NACA and RAE. In each figure, the intersections between the constraint bound and the constraint function signify the locations of the design feasibility boundaries along the direction ΔX. The vertical dotted lines have been added to illustrate that the feasibility boundaries coincide exactly with the optimal solutions at $\beta = 0$ and $\beta = 1$ for Cases NACA and RAE. For each solution, a step in either the positive or negative ΔX direction will result in an increase in the objective function or violation of one or more of the constraints.

Table 8 A comparison of performance values at two locally optimal solutions

Operating	Optimized NACA 0012 airfoil					Optimized RAE 2822 airfoil				
Point	α	C_l	C_d	M_{ks}	$C_{l,\max}$	α	C_l	C_d	M_{ks}	$C_{l,\max}$
A	−1.82°	0.17	0.0093	——	——	−1.44°	0.17	0.0093	——	——
B	−1.16°	0.28	0.0096	——	——	−0.81°	0.28	0.0095	——	——
C	−1.22°	0.27	0.0104	——	——	−0.86°	0.27	0.0103	——	——
D	−0.11°	0.45	0.0120	——	——	+0.19°	0.45	0.0110	——	——
E	−1.50°	0.21	0.0093	——	——	−1.18°	0.21	0.0093	——	——
F	−0.46°	0.36	0.0096	——	——	−0.16°	0.36	0.0096	——	——
G	−0.59°	0.34	0.0106	——	——	−0.28°	0.34	0.0106	——	——
H	+1.00°	0.57	0.0117	——	——	+1.28°	0.57	0.0117	——	——
I	−1.02°	0.28	0.0148	1.45	——	−0.84°	0.28	0.0111	1.38	——
J	−1.86°	0.15	0.0120	1.49	——	−1.50°	0.15	0.0117	1.43	——
K	+0.40°	0.46	0.0220	1.50	——	+0.19°	0.46	0.0145	1.44	——
L	−1.23°	0.25	0.0140	1.44	——	−0.99°	0.25	0.0110	1.38	——
M	+0.30°	0.45	0.0222	1.50	——	+0.13°	0.45	0.0150	1.43	——
N	−1.29°	0.24	0.0145	1.44	——	−1.04°	0.24	0.0118	1.38	——
O	+2.76°	0.74	0.0343	1.50	——	+1.79°	0.74	0.0226	1.50	——
P	−0.13°	0.40	0.0199	1.49	——	−0.16°	0.40	0.0138	1.41	——
Q	+14.64°	——	——	——	1.60	+14.65°	——	——	——	1.60
R	+14.64°	——	——	——	1.60	+14.41°	——	——	——	1.60

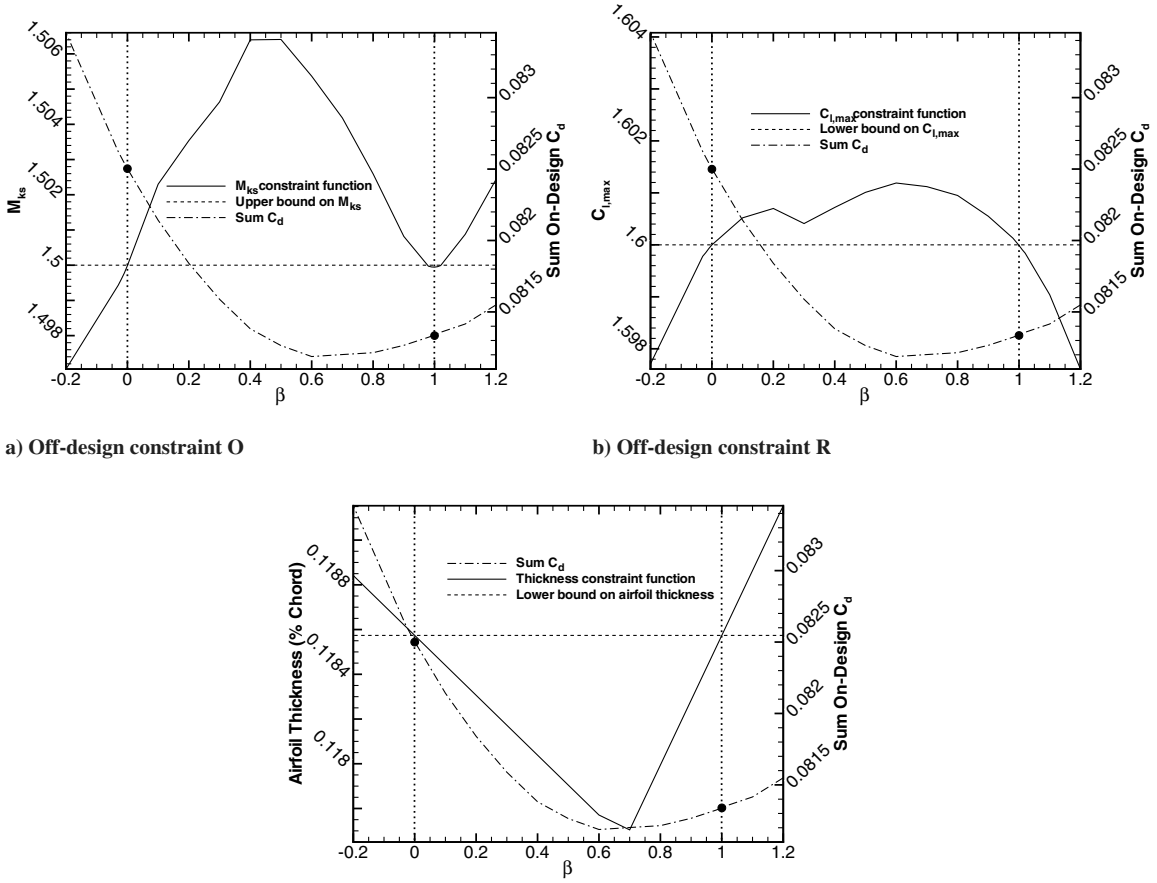

a) Off-design constraint O

b) Off-design constraint R

c) Airfoil thickness constraint

Fig. 16 Relationship between objective function and active constraints at solutions for cases NACA and RAE.

VIII. Conclusions

Two methods for solving practical aerodynamic design problems with competing design objectives and aerodynamic constraints using multipoint optimization have been presented. Both methods address issues that arise in practical multipoint optimization due to the coexistence of on-design and off-design points. The application of the off-design weight update method to an 18-point airfoil optimization demonstrates that it is able to adjust off-design weights iteratively based on the evolution of aerodynamic performance so as to satisfy off-design constraints while minimizing the penalty in on-design performance. The method allows designers to identify redundant and critical operating points. Furthermore, this technique is capable of preventing the off-design constraints from being oversatisfied to minimize their negative influence on the on-design performance. The resulting optimized airfoil for the baseline case satisfies all off-design constraints and minimizes degradation in on-design performance.

The second method using the constrained optimization algorithm SNOPT is capable of producing the same results as the off-design weight update method with significantly less computational effort. The off-design weight update method provides the opportunity to delete redundant operating conditions on-the-fly, thus potentially improving its computational efficiency.

Results presented in Sec. VII.F provide evidence for the existence of two locally optimal solutions to the practical aerodynamic design problem. Designers should be aware that more than one optimal solution is possible with design problems involving complex interactions between multiple objectives and constraints. Alternative optimization techniques, such as hybrid methods combining gradient-based and gradient-free approaches, may be appropriate for such problems.

The concept of design under uncertainty recognizes that various uncertainties involved in the optimization procedure can lead to significant uncertainty in the optimal solution. To further increase the usefulness of the approach presented here, it would be beneficial to incorporate a methodology for dealing with uncertainty.

Acknowledgments

The funding of the first and second authors by the Natural Sciences and Engineering Research Council of Canada and the third author by the Natural Sciences and Engineering Research Council of Canada and the Canada Research Chairs program is gratefully acknowledged.

References

[1] Li, W., Krist, S., and Campbell, R., "Transonic Airfoil Shape Optimization in Preliminary Design Environment," *Journal of Aircraft*, Vol. 43, No. 3, May–June 2006, pp. 639–651.

[2] Epstein, B., Jameson, A., Peigin, S., Roman, D., Harrison, N., and Vassberg, J., "Comparative Study of Three-Dimensional Wing Drag Minimization by Different Optimization Techniques," *Journal of Aircraft*, Vol. 46, No. 2, March–April 2009, pp. 526–541.

[3] Cliff, S. E., Reuther, J. J., Saunders, D. A., and Hicks, R. M., "Single-Point and Multipoint Aerodynamic Shape Optimization of High-Speed Civil Transport," *Journal of Aircraft*, Vol. 38, No. 6, Nov.–Dec. 2001, pp. 997–1005.

[4] Zingg, D. W., and Elias, S., "Aerodynamic Optimization Under a Range of Operating Conditions," *AIAA Journal*, Vol. 44, No. 11, Nov. 2006, pp. 2787–2792.
doi:10.2514/1.23658

[5] Li, W., Huyse, L., and Padula, S., "Robust Airfoil Optimization to Achieve Consistent Drag Reduction Over a Mach Range," *Struc-*

tural and Multidisciplinary Optimization, Vol. 24, No. 1, 2002, pp. 38–50.
doi:10.1007/s00158-002-0212-4

[6] Li, W., and Padula, S., "Using High Resolution Design Spaces for Aerodynamic Shape Optimization Under Uncertainty," NASA, Technical Rept. TP-2004-213003, 2004.

[7] Zingg, D. W., and Billing, L., "Toward Practical Aerodynamic Design Through Numerical Optimization," *18th AIAA Computational Fluid Dynamics Conference*, AIAA Paper 2007-4333, June 2007.

[8] Nemec, M., and Zingg, D. W., "Newton-Krylov Algorithm for Aerodynamic Design Using the Navier-Stokes Equations," *AIAA Journal*, Vol. 40, No. 6, June 2002, pp. 1146–1154.
doi:10.2514/2.1764

[9] Nemec, M., Zingg, D. W., and Pulliam, T. H., "Multipoint and Multi-Objective Aerodynamic Shape Optimization," *AIAA Journal*, Vol. 42, No. 6, June 2004, pp. 1057–1065.
doi:10.2514/1.10415

[10] Nocedal, J., and Wright, S., *Numerical Optimization*, 2nd ed., Springer–Verlag, New York, 2006.

[11] Gill, P. E., Murray, W., and Saunders, M. A., "SNOPT: An SQP Algorithm for Large-Scale Constrained Optimization," *Society for Industrial and Applied Mathematics Review*, Vol. 47, No. 1, Feb. 2005, pp. 99–131.
doi:10.1137/S0036144504446096

[12] Kreisselmeier, G., and Steinhauser, R., "Systematic Control Design by Optimizing a Vector Performance Index," *International Federation of Active Controls Symposium on Computer-Aided Design of Control Systems*, Zurich, Switzerland, Aug. 1979.

[13] Wrenn, G. A., "An Indirect Method for Numerical Optimization Using the Kreisselmeier-Steinhauser Function," NASA, Technical Rept. CR-4220, 1989.

[14] Anderson, W. K., and Bonhaus, D. L., "Airfoil Design On Unstructured Grids for Turbulent Flows," *AIAA Journal*, Vol. 37, No. 2, 1999, pp. 185–191.
doi:10.2514/2.712

[15] Martins, J. R. R. A., Alonso, J. J., and Reuther, J. J., "High-Fidelity Aerostructural Design Optimization of a Supersonic Business Jet," *Journal of Aircraft*, Vol. 41, No. 3, 2004, pp. 523–530.
doi:10.2514/1.11478

[16] Poon, N. M. K., and Martins, J. R. R. A., "An Adaptive Approach to Constraint Aggregation Using Adjoint Sensitivity Analysis," *Structural and Multidisciplinary Optimization*, Vol. 34, No. 1, 2007, pp. 61–73.
doi:10.1007/s00158-006-0061-7

[17] Stettner, M., and Schrage, D. P., "An Approach to Tiltrotor Wing Aeroservoelastic Optimization," *4th Symposium on Multidisciplinary Analysis and Optimization*, AIAA, Reston, VA, 1992.

[18] Zingg, D. W., "Grid Studies for Thin-Layer-Navier–Stokes Computations of Airfoil Flowfields," *AIAA Journal*, Vol. 30, No. 10, 1992, pp. 2561–2564.
doi:10.2514/3.11265

[19] Zingg, D. W., De Rango, S., Nemec, M., and Pulliam, T. H., "Comparison of Several Spatial Discretizations for the Navier–Stokes Equations," *Journal of Computational Physics*, Vol. 160, No. 2, May 2000, pp. 683–704.
doi:10.1006/jcph.2000.6482